IMPLEMENTATION AND VALIDATION OF A METHOD TO INTRODUCE SYNTHETIC TURBULENCE BY VOLUME FORCES

EIKE TANGERMANN[1], MARKUS KLEIN[2]
[1]*Universität der Bundeswehr München, eike.tangermann@unibw.de*
[2]*Universität der Bundeswehr München, markus.klein@unibw.de*

Keywords: *Synthetic turbulence, turbulence-resolving methods, LES, DES*

In CFD simulations from the field of external aerodynamics the usage of boundaries of the farfield type is very common. In such configurations the boundary is located far away from the region of interest in order to decouple the boundary conditions from the phenomena in the vicinity of the geometry under investigation. Grid cells outside of the focus region are usually significantly increasing in size since small flow structures are either not present or not desired. This method is suitable for both steady and unsteady investigations.
However, when investigating the interaction of the flow field with perturbations in the approaching flow the problem arises to transport the perturbation towards the focus region. Such perturbations can for example represent a gust of larger scale or resolved turbulent fluctuations of several, usually smaller, scales. The convective transport from the inflow boundary requires a significantly higher grid resolution in order to resolve the perturbations and also a long span of computed time at a time step size sufficiently low to preserve details of the fluctuations.
Several approaches have been introduced to circumvent this issue by introducing the perturbations closer to the focus region. Recently Schmidt and Breuer [1] have proposed a method based on applying a volume force to superimpose synthetic turbulence at arbitrary locations of the computational domain.
The present work features the implementation of a method, which adapts the approach by Schmidt and Breuer, in the pimpleFoam solver. As in the original publication a source term F^{syn} representing a volume force is added to the momentum equation. It is present only in those regions, where the fluctuations are to be superimposed to the mean velocity field. Schmidt and Breuer propose to generate the fluctuation field according to Klein et al. [2] from digital filtering of a random field. However, other methods might also be used. Here a similar approach has been selected and implemented in OpenFOAM, in which the filtering is achieved by solving a diffusion equation [3].
With the force term the momentum equation becomes

$$\frac{\partial \vec{u}}{\partial t} + \nabla \cdot (\vec{u}\vec{u}) - \nabla \cdot (\nu \nabla \vec{u}) = -\nabla p + \vec{F}^{syn}. \tag{1}$$

The force needs to be set appropriately in order to achieve the desired velocity fluctuations. The location of a forcing zone upstream of an airfoil is shown in Figure 1. As in the original publication the force field is not moving continuously with the convection velocity. Instead one slice from the fluctuation field is used for the entire forcing region being updated every time step.
The volume force depends primarily on the transition time T a fluid element spends travelling across the influence region. To facilitate the numerical solution the force should not introduce sudden jumps into the equation. Therefore a Gaussian bell-shaped function G is introduced to smoothen the force field towards its boundaries. To preserve the total force effect G ist normalized by its mean value $\overline{G}$. Assuming that the undisturbed flow primarily is pointing in the x-direction, the force term superimposing a fluctuation velocity $(u')^{syn}$ is calculated by

$$F_{syn} = \frac{(u')^{syn}}{T} \cdot G(x,y,z)/\overline{G} = \frac{(u')^{syn}}{L_x/u_0} \cdot G(x,y,z) \cdot \left(1/L_x \int_{-L_x/2}^{L_x/2} G(x)\, dx \right)^{-1}. \tag{2}$$

At weak levels of turbulence intensity the bell function primarily acts in the flow direction. For stronger turbulence it can become necessary to smoothen the force field towards all edges of the forcing region. Thus a three-dimensional function is applied.

$$G = \exp\left(-\frac{\pi}{2} \left(\frac{(x-x_0)^2}{(L_x/2)^2} + \frac{(y-y_0)^2}{(L_y/2)^2} + \frac{(z-z_0)^2}{(L_z/2)^2} \right) \right) \tag{3}$$

This modification of the momentum equation needs to be taken into account in the pressure equation. In the semi discretized form according to Jasak [4] an additional term arises.

$$\nabla \cdot \left(\frac{1}{a_p} \nabla p \right) = \nabla \cdot \left(\frac{H(\vec{u})}{a_p} \right) + \nabla \cdot \vec{F}^{syn} \tag{4}$$

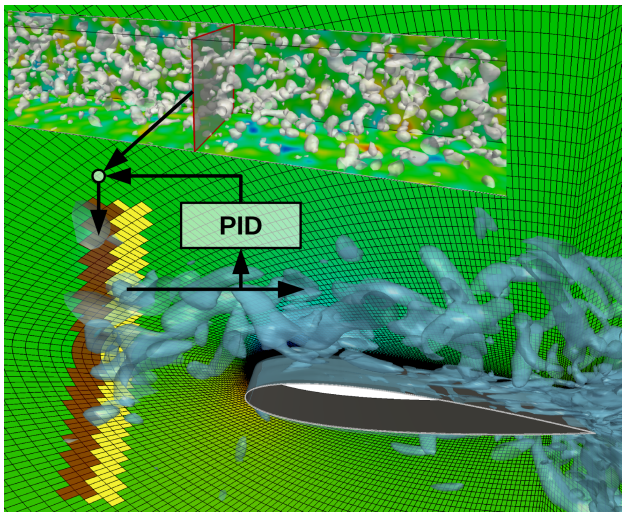

Figure 1: Setup of forcing and controller. The synthetic fluctuations are introduced in the red forcing region, the resulting fluctuation velocity is then determined in the yellow control region and looped back via the PID controller.

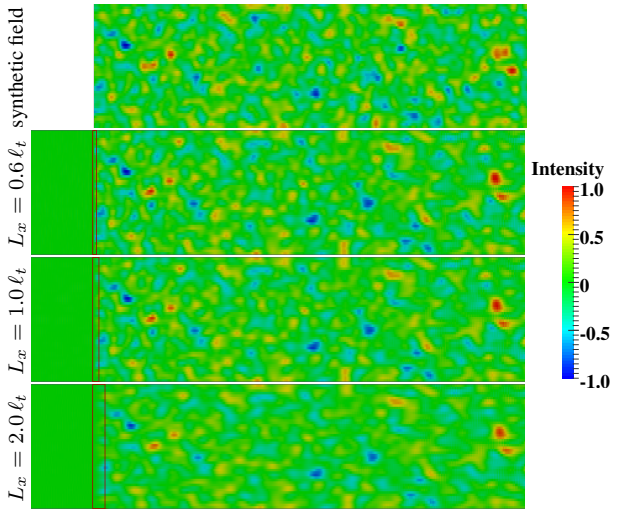

Figure 2: Original fluctuation field (top) and transport as a passive scalar with variations of L_x. Decreasing intensity of small scale fluctuations with increasing width.

a_p denotes the matrix coefficient for the central cell and $H(\vec{u})$ represents the neighbour cells and the temporal derivative. It needs to be mentioned that, if the forcing term in the momentum equation is implemented correctly in OpenFOAM, $H(\vec{u})$ will also incorporate it as a source term. However, this has been prevented here for the sake of demonstration.
As mentioned before one slice of the fluctuation field is spread along the forcing region. This means, that the local force changes, while a fluid element is passing. This changes the amount of force applied depending on the ratio of the length scale of each fluctuation to the forcing region length. The wider the forcing zone is selected the lower the fluctuation amplitude will become. This is illustrated in Figure 2 with fluctuations of a passive scalar field, for which a convection equation with constant convection velocity has been solved. It shows the field of synthetic fluctuations in the upper image and below the field for different widths of the forcing region. While the length scale of the fluctuations is produced very well, the magnitude especially of the smaller eddies decays with increasing width of the forcing region.
To overcome this a control loop is used inspired by the mechanism proposed in [5]. An amplification factor is introduced in Equation 2, which scales the force field globally. Downstream of the forcing region a control region needs to be placed, in which the resulting fluctuation velocity or turbulent kinetic energy is calculated. In order to reduce local variations of turbulence intensity the control region should be set sufficiently wide, then the mean value of u'_{rms} is calculated inside. The difference between the actual and desired fluctuation velocity, the error variable $e = u'_{target} - u'_{rms}$, is determined. The calculated error is then processed in a common PID control function in a discrete formulation.

$$u_{c,n} = K_p \cdot e_n + K_i \sum_{0}^{n} e_n \Delta t_n + K_d \frac{e_n - e_{n-1}}{\Delta t_n}. \tag{5}$$

The controller output u is then added to the amplification factor. For the calculations in the present study a set of $K_p = 1.0$, $K_i = 0.0001$ and $K_d = 0.1$ has been selected for the controller coefficients ensuring stability and sufficiently fast reaction time. However, these values depend strongly on the dead time in the control loop.
With this controller mechanism the magnitude of the input fluctuation field becomes irrelevant. Only the length scale and, if required, the cross correlation of the Reynolds stresses need to be prescribed correctly. The magnitude of the fluctuations can then be amplified to an arbitrary value.
To demonstrate this capability the two-dimensional flow around a cylinder with synthetic fluctuations in the approaching flow has been calculated with different settings for the turbulence intensity. The setup is shown in Figure 3, the forcing zone is located one diameter upstream of the cylinder and 1.5 times the diameter downstream of the inlet boundary. It extends up to five cells in stream-wise direction. The measuring region of the controller is located immediately downstream of the forcing.
From one field of synthetic fluctuations calculations at four different turbulence levels have been performed. They range from from almost undisturbed flow ($u'_{rms}/u_\infty = 0.01$) to high turbulence ($u'_{rms}/u_\infty = 1$). At a Reynolds-number of $2 \cdot 10^5$ based on the undisturbed flow velocity and diameter the cylinder wake flow forms a characteristic Karman vortex street, which is perturbed by the approaching fluctuations. An instantaneous view to the flow field is given by Figure 4 for two settings of turbulence intensity after sufficient computed time to achieve a quasi-steady state. The smaller scale eddies become dissipated quickly downstream of the cylinder because of dissipation and coarser mesh resolution.
The controller reaches the prescribed turbulence level approximately within five characteristic time units (CTU). As illustrated in Figure 5 an overshoot occurs and around fifteen CTU the final level of amplification is reached. In the case

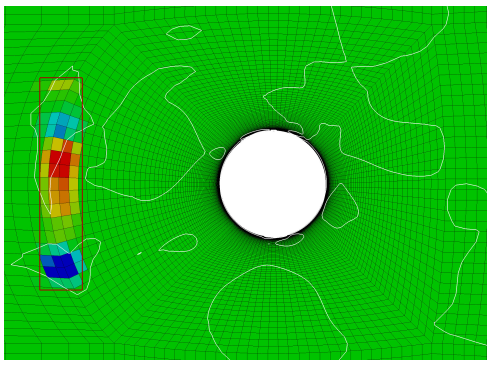

Figure 3: Instantaneous volume force field F_x^{syn} and isolines of Q.

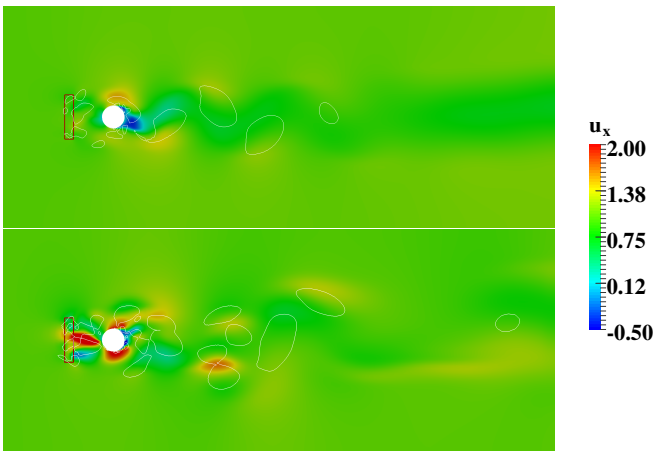

Figure 4: Cylinder flow with synthetic turbulence. $u'/u_\infty = 0.1$ (top) and $u'/u_\infty = 0.5$ (bottom). White isolines from Q-criterion.

with lowest turbulence intensity the setup fails, the amplification factor drops to zero (where it is bounded) after fifteen CTU. The reason is, that the vortex street induces very small variations of the velocity upstream of the cylinder. These are recorded by the controller and in this case they are sufficient to pretend the presence of enough synthetic fluctuations. To overcome this, the mechanism would have to be placed further upstream of the cylinder, where no influence of the vortex street is measurable. This means, that this case is almost identical with a case without perturbation.

The effect of turbulence in the approaching flow is, that the vortex street forms sooner. Figure 6 shows the temporal evolution of the lift coefficient. In the case with the lowest turbulence the longest time is needed to achieve the final amplitude of the alternating vortex separation. In the second case the development of the vortex street happens sightly sooner and it then reaches its final amplitude after a short time. The appearance of the lift curve still is regular with only slight perturbations.

In the third case the separation starts almost immediately compared to the previous two cases. The influence of the perturbation is clearly visible but also the characteristic of the alternating separation remains visible in the lift plot. In the case of highest turbulence intensity the alternating pattern almost vanishes while the force is dominated by the perturbations. The coefficient reaches values far higher than those seen purely from the vortex street. The velocity field shows, that the vortex street is still present but it is strongly deformed by the perturbations.

In order to determine the significance of the changes to the pressure equation the same set of cases has been calculated again with the original pressure equation and the forcing term only being present in the momentum equation. As long as the iterative procedure of the PIMPLE algorithm converges, this is supposed to reach the same converged state for each time step as in the previous setup but might need more corrective iteration steps for the pressure equation. The result of the comparison is presented in Table 1.

For all four cases the computing time and the number of pressure equations are compared. The data is taken from a calculation at quasi-steady state simulating a range of five CTU starting after the first twenty CTU. In the first case it needs to be reminded, that the controller mechanism has faded out the turbulent forcing for most of the time. This still produces overhead to handle the zero-forcing in the pressure equation and leads to an increase of computing time. However, the number of pressure iterations decreases during the short phases, when the amplification becomes greater than zero. This resuts in a slight decrease in total pressure iterations.

For the three cases with significant perturbation level the result changes considerably. The number of pressure iterations decreases by more than ten percent and up to thirteen percent. The reduction of computing time is not as big as the

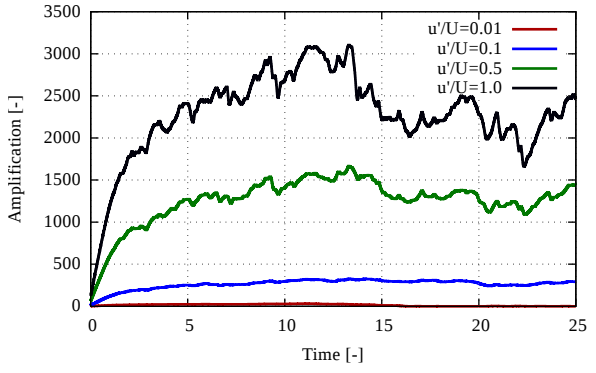

Figure 5: Amplification factor from the controller for different turbulence intensities.

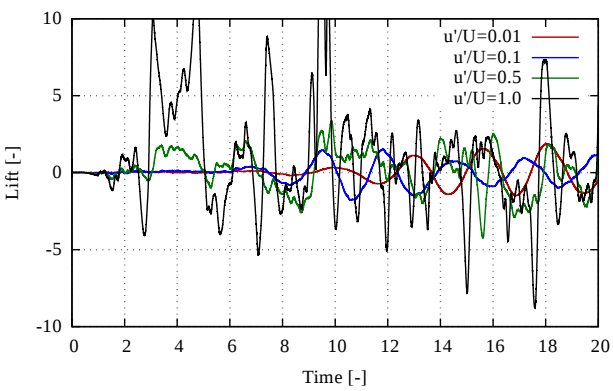

Figure 6: Cylinder lift coefficient.

Table 1: Relative change in computational effort with corrected pressure equation.

$\mathbf{u'_{rms}/u_\infty}$	Computing Time	Pressure Iterations
0.01	+3.5%	–0.63%
0.1	–6.0%	–13.3%
0.5	–7.8%	–11.5%
1.0	–7.0%	–10.4%

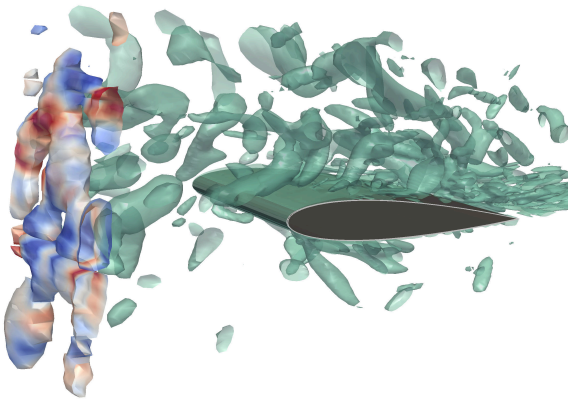

Figure 7: Flow around a NACA0012 airfoil. Q isosurfaces (green) and volume force (red/blue).

decrease of pressure iterations but still significant. It ranges from six to almost eight percent. It appears to be independent of the fluctuation magnitude. However, the difference for each case certainly has a strong dependence on the solver settings and can vary for different applications.

The two-dimensional cases presented here have been selected to reduce computational effort for validation and demonstration. Actual turbulence needs to be studied in three-dimensional applications to resolve the three-dimensional aspect of turbulent motion correctly. Such turbulence-resolving computations require parallelisation to achieve results within reasonable computing wall time. It should be noted, that in a parallel computation the controller needs intercommunication to produce one uniform amplification factor.

As a three-dimensional test case the flow around a NACA0012 airfoil is shown here. It is a hybrid RANS LES simulation featuring the kωSST-DDES model. The Reynolds-number is 50000 and the flow is approaching the airfoil at an angle of attack of six degrees. The mesh of 2.5 million hexahedral cells extends half the chord length in span-wise direction with a periodic boundary condition and has a structured C topology. The computational domain extends 20 times the chord length from the leading edge, on the outer side it features a farfield boundary condition. Here it would not be possible to prescribe turbulence at the inflow boundary. Instead perturbations are introduced half a chord length upstream of the leading edge.

The prescribed turbulence features an intensity of $u'/u_\infty = 0.1$ and its integral length scale is one tenth of the chord length. The initial amplification is set too high and after one CTU the correct level of amplification is reached. In case of laminar inflow this simulation will not show any resolved turbulent motion. The turbulence model acts in RANS mode along the wall not resolving boundary layer turbulence. This leads to a steady and smooth flow. With turbulence in the approaching flow the vortices reaching the airfoil produce fluctuations of the aerodynamic forces and moments. The isosurfaces of Q in Figure 7 illustrate the vortices passing around the airfoil and perturbing the boundary layer.

Under circumstances, where the flow tends to separate, the approaching turbulence can significantly affect the separation behaviour of the flow. This will be subject of forthcoming investigations within the field of laminar separation.

Concluding the presented work, the implementation of the method to introduce synthetic turbulence at arbitrary locations within the computational domain can be considered validated. By considering the volume force in the pressure equation a significant reduction of computational effort has been achieved. Finally a controller mechanism has been introduced to compensate the distortion of the perturbation amplitude. This further allows to easily scale a field of synthetic fluctuations to other levels of turbulence intensity. The method has been shown to be working in two- and three-dimensional cases as well as in parallel computations.

References

[1] S. Schmidt and M. Breuer, "Source term based synthetic turbulence inflow generator for eddy-resolving predictions of an airfoil flow including a laminar separation bubble," *Computers & Fluids*, vol. 146, pp. 1–22, 2017.

[2] M. Klein, A. Sadiki, and J. Janicka, "A digital filter based generation of inflow data for spatially developing direct numerical or large eddy simulations," *Journal of computational Physics*, vol. 186, no. 2, pp. 652–665, 2003.

[3] A. Kempf, M. Klein, and J. Janicka, "Efficient generation of initial-and inflow-conditions for transient turbulent flows in arbitrary geometries," *Flow, Turbulence and combustion*, vol. 74, no. 1, pp. 67–84, 2005.

[4] H. Jasak, "Error analysis and estimation for finite volume method with applications to fluid flow," 1996.

[5] M. Klein, N. Chakraborty, and S. Ketterl, "A comparison of strategies for direct numerical simulation of turbulence chemistry interaction in generic planar turbulent premixed flames," *Flow, Turbulence and Combustion*, vol. 99, no. 3-4, pp. 955–971, 2017.